Bull. Mater. Sci., Vol. 36, No. 2, April 2013, pp. 223–229. © Indian Academy of Sciences.

Preparation of manganese-doped ZnO thin films and their characterization

S MONDAL, S R BHATTACHARYYA[†] and P MITRA[*]
Department of Physics, University of Burdwan, Golapbag, Burdwan 713 104, India
[†]Surface Physics Division, Saha Institute of Nuclear Physics, Kolkata 700 064, India

MS received 8 January 2012; revised 21 March 2012

Abstract. **In this study, pure and manganese-doped zinc oxide (Mn:ZnO) thin films were deposited on quartz substrate following successive ion layer adsorption and reaction (SILAR) technique. The film growth rate was found to increase linearly with number of dipping cycle. Characterization techniques of XRD, SEM with EDX and UV–visible spectra measurement were done to investigate the effect of Mn doping on the structural and optical properties of Mn:ZnO thin films. Structural characterization by X-ray diffraction reveals that polycrystalline nature of the films increases with increasing manganese incorporation. Particle size evaluated using X-ray line broadening analysis shows decreasing trend with increasing manganese impurification. The average particle size for pure ZnO is 29·71 nm and it reduces to 23·76 nm for 5% Mn-doped ZnO. The strong preferred *c*-axis orientation is lost due to manganese (Mn) doping. The degree of polycrystallinity increases and the average microstrain in the films decreases with increasing Mn incorporation. Incorporation of Mn was confirmed from elemental analysis using EDX. As the Mn doping concentration increases the optical bandgap of the films decreases for the range of Mn doping reported here. The value of fundamental absorption edge is 3·22 eV for pure ZnO and it decreases to 3·06 eV for 5% Mn:ZnO.**

Keywords. **SILAR; Mn:ZnO thin film; X-ray line broadening; SEM; optical bandgap.**

1. Introduction

Zinc oxide is a II–IV semiconductor compound and has a large direct bandgap around 3·2–3·37 eV at 300 K with a high exciton binding energy of 60 meV (Nirmala and Anukaliani 2010). ZnO thin films are important materials due to their unique properties such as piezoelectricity, chemical stability, biocompatibility, high catalytic activity in different gas ambient, high optical transparency in the visible region and high voltage-current nonlinearity etc. (Look 2001; Keis *et al* 2002; Maiti *et al* 2007). Accordingly it has an immense potential in different applications in photo-thermal conversion systems, heat mirrors, hetero-junction solar cells, transparent electrodes, blue/UV-light emitter device, solid state sensor, transducer, etc. (Wang *et al* 1995; Natsume 2000; Negami *et al* 2001). Pure zinc oxide thin films have certain limitations in their application. In order to widen the potential areas where ZnO thin films can be applied, dopant ions have to be incorporated into them to obtain certain desired properties like wider or narrower bandgap, higher optical absorbance, lower or higher melting point, ferromagnetism, etc. Mn-doped ZnO has the potential to be a multifunctional material with coexisting magnetic, semi-conducting and optical properties (Mandal and Nath 2006). It is regarded as promising material for spintronic applications as it shows room temperature ferromagnetism (Singhal *et al* 2009). Thus Mn-doped ZnO has been synthesized primarily to study its ferromagnetic behaviour (Sharma *et al* 2003; Kundaliya *et al* 2004). Due to its unique magneto-optical, magneto-electrical and magneto-transport properties, it is also considered as a dilute magnetic semiconductor (DMS) material. Various physical and chemical techniques that has been used to deposit Mn:ZnO thin films and nanofilms includes rf or d.c. sputtering, pulsed-laser deposition (PLD), ion plating, chemical vapour deposition (CVD), thermal evaporation, spray pyrolysis, molecular beam epitaxy (MBE), etc. (Nirmala and Anukaliani 2010). Chemical techniques are relatively simpler and cost effective.

In the present work, an attempt has been made to synthesize Mn-doped ZnO thin films by a chemical dipping technique. In this technique, a glass substrate is dipped alternately into beakers containing aqueous solutions or distilled water for the reaction to take place at the substrate surface. The substrate can be introduced into various reactants for a specific length of time depending on the nature and kinetics of the reaction. The immersion-reaction cycle can be repeated for any number of times, limited only by the inherent problems associated with the deposition technique and the substrate–thin film interface. The technique is called SILAR (successive ion layer adsorption and reaction) since it involves adsorption of a layer of complex ion on the substrate followed by the reaction of the adsorbed ion layer.

[*]Author for correspondence (mitrapartha1@rediffmail.com)

Thus SILAR is one such process which is based on successive irreversible acts of adsorption of cations and then anions. Since the synthesis can be carried out under 'mild conditions' and at lower processing temperatures, implantation of metal ions at low temperatures may be particularly suitable by this method. Lower processing temperature also prevents the films from considerable loss of their intrinsic electrical and optical properties as well. The SILAR deposition from aqueous solutions is a very promising method because of its simplicity and economy. The technique is, however, a relatively less used and studied one and there are no reports of synthesis of Mn:ZnO thin films by SILAR. The advantages of this method are its simplicity of working principle and low cost of apparatus. Earlier we have reported the synthesis of ZnO, aluminum and cadmium-doped ZnO (Mitra and Khan 2006; Mondal *et al* 2008; Mondal and Mitra 2012) thin films by SILAR. The primary aim of the present work was to explore the possibility of utilizing SILAR to impurify ZnO thin film with Mn.

2. Experimental

Deposition of pure ZnO film was carried out from 0·1 M zinc chloride ($ZnCl_2$) solution kept at room temperature and 0·075 M sodium hydroxide (NaOH) solution maintained at 70 °C. Commercially available quartz substrate was used for film deposition. The substrate was cleaned before deposition, by etching in 1% hydrofluoric acid (HF) for 24 h followed by ultrasonic cleaning in equivolume acetone and alcohol and thorough rinsing in deionized water. The cleaned substrate was alternatively dipped in zinc chloride solution and hot NaOH solution. One complete set of dipping cycle involves dipping in zinc chloride bath for 2 s and dipping in sodium hydroxide bath for 2 s. For Mn doping, manganese (II) chloride ($MnCl_2 \cdot 4H_2O$, Merck, mol. wt. 197·9) dissolved in zinc chloride solution was used as a source of Mn^{2+} dopant ions. The manganese concentration was varied up to 5% in the zinc chloride solution for the preparation of doped films. Film thickness was measured using gravimetric weight difference method (Kale *et al* 2007; Mondal and Mitra 2012).

The X-ray diffraction profiles of the pure and doped samples were recorded using Ni-filtered CuK_α radiation from a highly stabilized and automated Philips X-ray generator (PW 1830) operated at 40 kV and 20 mA. The experimental peak positions were compared with the standard JCPDS files and the Miller indices were indexed to the peaks. Scanning electron microscopy (SEM, Model S530, Hitachi, Japan) was used to study the surface morphology and to illustrate the formation of crystallites on the film surface. Energy dispersive X-ray analysis (EDX) was employed for the compositional analysis. UV–Vis spectrophotometer measurements were performed by using a spectrophotometer (Shimadzu, UV-1800) at room temperature. The spectra were recorded by using a similar quartz substrate as a reference and hence the absorption due to the film only was obtained. The bandgap of the films has been evaluated from the absorption edge of the spectrum.

3. Results and discussion

3.1 *Film deposition and thickness measurement*

The zinc chloride bath, used for deposition was prepared by adding zinc chloride in deionized water. 6·814 gm zinc chloride ($ZnCl_2$, Merck, mol. wt. 136·28) was added in 500 cc deionized water to have a bath solution of 0·1 M $ZnCl_2$. One of the problems with zinc chloride solution is that complete dissolution of the solute does not occur and precipitate appears on standing. Addition of three drops of acetic acid (∼0·3 cc by volume) gives a clear transparent solution. The pH of the transparent solution was 4·70. pH measurement was carried out in a Systronics pH meter (Model 335). 0·075 M sodium hydroxide solution was prepared by dissolving NaOH pellets (Merck, mol. wt. 40) in 500 cc deionized water. The pH of the sodium hydroxide bath was 11·10. The concentrations of the reacting baths used were found to be optimum for synthesis of good quality adherent film. For concentrations more than 0·125 M for zinc chloride bath and/or for concentrations more than 0·075 M for sodium hydroxide bath, particulate absorption took place on the film surface making the growth process nonuniform and resulting in poor quality films. For still higher concentrations of either bath, film detachment from the substrate surface takes place and no layer could be deposited. The film thickness (t) was built up by increasing the number of dipping cycle. The deposited films were subsequently annealed in air at 350 °C for 2 h. Figure 1 shows the dependence of film thickness on the number of dipping cycles (N). The film thickness was determined gravimetrically by measuring the change in weight of the substrate due to film deposition,

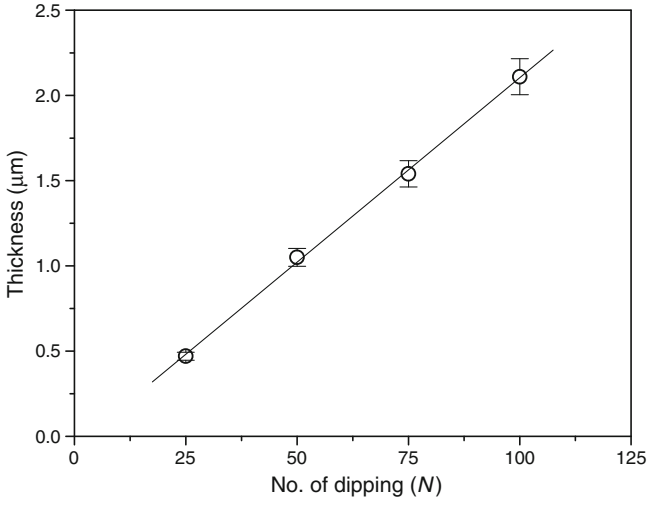

Figure 1. Dependence of film thickness on number of dipping cycles.

the area of deposition and using the known density of ZnO (5·6 gm/cm^3). Thus, if W_1 and W_2 are the weights of the substrate before and after film deposition in g, A is the area of film deposition in cm^2 and ρ is the theoretical density of ZnO, then the film thickness is evaluated as:

$$d = \frac{(W_2 - W_1)}{A\rho} \times 10^{-4} \mu\text{m}.$$

It is seen from figure 1 that the film thickness follows a linear growth law with number of dipping cycle and the growth rate was found to be 0·021 μm/dipping for pure ZnO film measured gravimetrically. There is an overall variation of ±5% in the film thickness data (shown as error bars against each data point of figure 1). This reflects a small variability in the deposition process arising probably from small experimental scatter in deposition parameters (e.g. bath concentration, bath temperature, etc.) as well as due to the nonuniformity of the substrate handling procedure as the deposition is carried out manually.

The growth rate was found to decrease with Mn incorporation. For 50 dipping, the film thickness for pure ZnO was 1·05 μm. The corresponding thickness for 2% Mn:ZnO film was 0·94 μm and for 5% Mn:ZnO, the thickness was 0·82 μm. Thus the growth rate decreases with increasing Mn incorporation. It was 0·021 μm/dipping for pure ZnO. It reduces to 0·0188 μm/dipping and 0·0164 μm/dipping for 2 and 5% Mn:ZnO, respectively. The ZnO film was white in appearance and Mn-doped films were slightly brownish with a good adherence to the substrate.

The film thickness was also checked against cross-sectional SEM. Some portion of the substrate was acid etched to remove film from that area in order to create a step for thickness measurement. Figure 2 shows cross-sectional SEM micrograph of undoped ZnO film of thickness 2·1 μm measured gravimetrically (obtained by 100 dipping). An average thickness of 2·56 μm was obtained from SEM micrograph. The value was an average of several measurements on different portions.

The gravimetric method does not take account of porosity in the films. As the films are porous in nature, the actual film density is always lower than the theoretical density. So the film thicknesses estimated using the theoretical density value is the minimum value and is always less than the actual thickness. The actual thickness determined from cross-sectional SEM is 22% higher than the gravimetric value (2·56 μm measured by TEM as opposed to 2·1 μm measured gravimetrically). This indicates a porosity of ~22% in the deposited films.

3.2 *Structural characterization*

The X-ray diffraction patterns of undoped ZnO and Mn-doped ZnO films are shown in figure 3. The diffractions pattern for undoped ZnO is shown in figure 3(a). Figures 3(b) and (c) show the diffractograms for 2 and 5% Mn:ZnO films, respectively. The films were heat treated at 350 °C for 2 h, prior to structural characterization. The materials were scanned in the range 25–65°. The 2θ variation was employed with a 0·05° step and a time step of 1 s. Intensity in arbitrary units is plotted against 2θ in figure 1. It is seen from figure 3(a) that peaks appear at 31·708, 34·397, 36·183, 47·516, 56·551 and 62·88°. The diffractogram of the sample reveals that all the peaks are in good agreement with the joint committee on powder diffraction standard (JCPDS) data belonging to hexagonal ZnO structure (Card No. 36-1451). The corresponding reflecting planes are (100), (002), (101), (102),

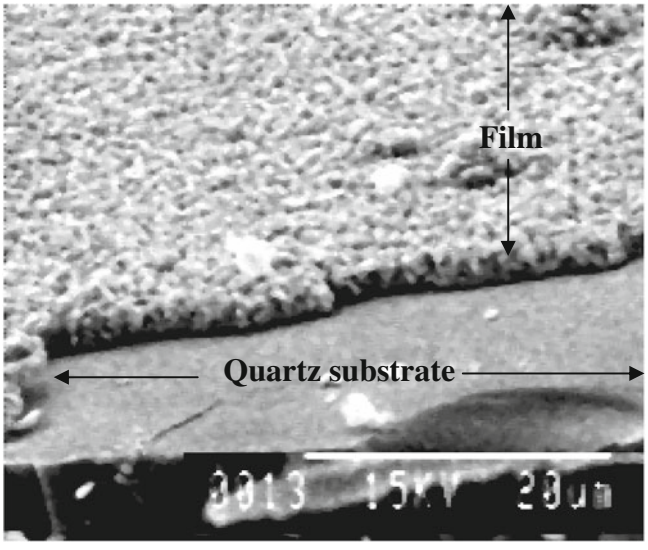

Figure 2. Cross-sectional SEM of undoped ZnO film.

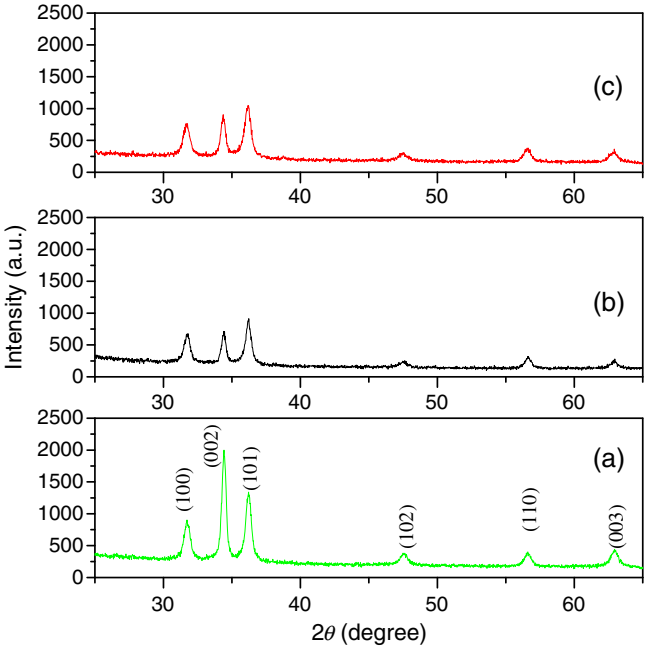

Figure 3. X-ray diffraction pattern of (**a**) ZnO, (**b**) 2% Mn:ZnO and (**c**) 5% Mn:ZnO.

(110) and (103), respectively. The (002) peak appears with maximum intensity at 34·397°. Apart from ZnO characteristic peaks, no extra peaks due to manganese clusters, zinc or their complex oxides could be detected. This observation suggests that the films are single phase and Mn ion might have substituted Zn site without changing the hexagonal structure.

It is evident from figure 3(a) that undoped ZnO film have a polycrystalline structure with preferred orientation mostly along the (002) diffraction plane. Compared to pure ZnO film, the intensity of (002) peak decreases for Mn:ZnO films. This results in an increase of relative intensity of (101) peak w. r. t. (002) peak. The (101) peak appears with maximum intensity in ZnO powders with no preferred orientation (Mitra and Khan 2006). Thus crystalline nature of films was affected due to enhancement of dopant concentration, by which manganese impurities were included in the ZnO crystal. Such loss of preferred orientation and crystalline nature with Mn incorporation has been reported by Nirmala and Anukaliani (2010). Doping results in loss of preferred orientation along *c*-axis. Utilizing the X-ray diffraction data, the average particle size was estimated from Williamson–Hall equation (Ungar and Borbely 1996; Choudhury and Sarma 2009).

$$\beta \cos\theta = \frac{k\lambda}{D} + 4\varepsilon \sin\theta, \tag{1}$$

where λ is the wavelength of radiation used (1·542 Å of CuK_α radiation used), k the Scherrer constant, β the full width at half maximum (FWHM) intensity of the diffraction peak for which the particle size is to be calculated, θ the diffraction angle of the concerned diffraction peak, D the crystallite dimension (or particle size) and ε the microstrain. In general, the experimentally observed X-ray peak broadening (β_o) is a convolution of (i) instrumental broadening; (β_i), (ii) particle (crystallite) size broadening (β_D) and (iii) lattice strain broadening (β_S). The total broadening due to size and strain (β) can be represented as $\beta = \beta_D + \beta_S$ and can be obtained from the experimentally observed broadening (β_o) using the equation (Klug and Alexander 1974; Patra *et al* 2011):

$$\beta = \beta_o - \beta_i. \tag{2}$$

Diffraction data from standard silicon (Si) powder was used to estimate the instrumental broadening (Sharma *et al* 2003; Patra *et al* 2011). The broadening (in FWHM) against 2θ obtained for standard silicon sample was plotted in a graph and was used as reference. The instrumental broadening at the observed peak positions for ZnO and Mn-doped ZnO was evaluated from the graph.

X-ray line broadening analysis to evaluate FWHM (β) was carried out using computer software (MARQ2) (Jumin and Wang 2001; Ghosh *et al* 2009). The software utilizes Marquardt least-squares procedure for minimizing the difference between the observed and simulated diffraction patterns. The peak shape and intensity of reflection is modeled with a pseudo-Voigt (pV) analytical function, which is a combination of a Gaussian and a Lorentzian functions. The background intensity is subtracted by fitting the background with a suitable linear function. A typical plot of MARQ2 analysis for 5% Mn:ZnO sample is shown in figure 4. The dotted curve represents the experimental intensity data (I_o) while the continuous curve represents the calculated (simulated) intensity data (I_c). The difference plot ($I_c - I_o$) is shown at the bottom of figure 4.

From the values of β_o obtained using MARQ2 fitting and the corresponding values of instrumental broadening, β_i, FWHM β was calculated using (2). Figure 5 shows the plot of $\beta\cos\theta$ ordinate against $4\sin\theta$ along abscissa (Williamson–Hall plots). The slope of the straight line plots represents average strain in the films whereas the inverse of intercept on $\beta\cos\theta$ axis gives the crystallite size (D)

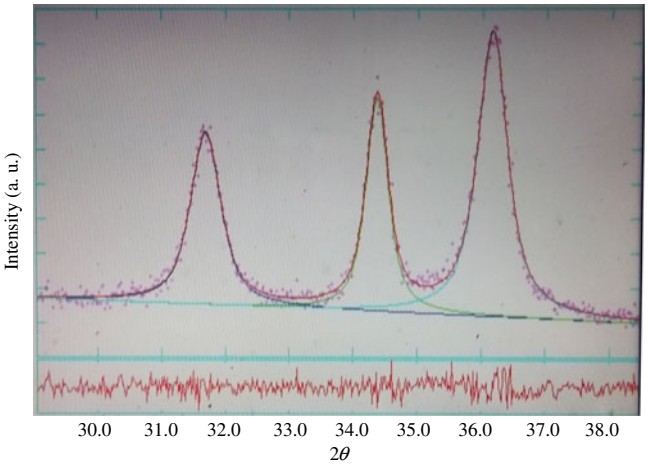

Figure 4. Observed (dotted) and simulated (continuous) X-ray diffraction patterns of 5% Mn:ZnO.

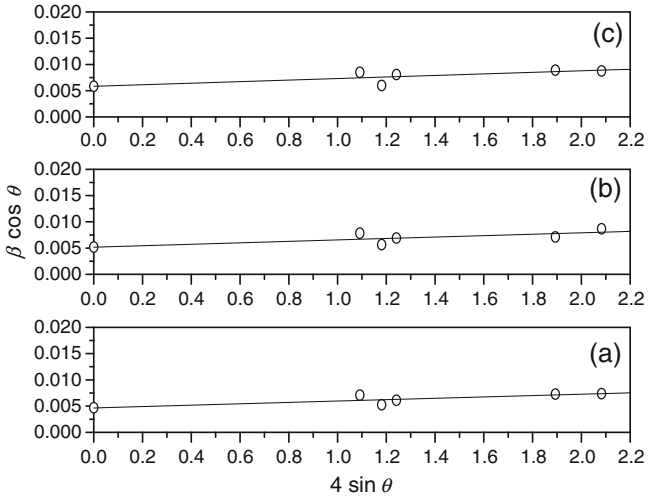

Figure 5. Williamson–Hall plots of (**a**) pure ZnO, (**b**) 2% Mn:ZnO and (**c**) 5% Mn:ZnO films.

according to (1). The particle size was evaluated using $k = 0{\cdot}9$, which corresponds to spherical crystallites and $\lambda = 1{\cdot}5418$ Å, the wavelength of CuK_α radiation. The average value of particle size for pure ZnO is 29·71 nm. It decreases to 26·79 nm for 2% Mn:ZnO and 23·76 nm for 5% Mn:ZnO. The average microstrain in the films as determined from W–H plots is 0·0013, 0·00137 and 0·00146, respectively for pure, 2% Mn:ZnO and 5% Mn:ZnO films, respectively. Thus the particle size decreases with increasing Mn incorporation and the strain increases. The decrease in average particle size with increasing Mn doping, i.e. hindrance of grain growth upon Mn incorporation has been reported by other workers (Luo *et al* 2005; Deka and Roy 2007; Senthilkumar *et al* 2008). The decrease in average particle size might be due to the development of strain in the films because of Mn incorporation. Such enhancement of average microstrain with Mn incorporation has been observed in the present work.

Figure 6 shows the HRSEM micrograph of pure ZnO film. HRSEM image shows structure consisting of many spherical shaped nanoparticles. The average particle size was found to be ~31 nm which matches well with that obtained using X-ray line broadening analysis. HRSEM study was undertaken in a FEI FEG Nova 600 Nanolab at 5 kV. Figure 7 shows the SEM image of 5% Mn:ZnO film. Surface morphology study of 5% Mn:ZnO films shows wrinkle structure with formation of nanorods in certain regions. Similar observation of appearance of wrinkle structure due to Mn incorporation has been reported by Nirmala and Anukaliani (2010). Srinivasan and Kumar (2008) were also reported microstructure consisting of nanorods with wrinkle structure for Mn-doped films.

The compositional analysis of Mn-doped ZnO film carried out by energy dispersive X-ray analysis is shown in figure 8. Figure 8(a) shows the EDX spectrum of 2% Mn:ZnO and figure 8(b) shows the spectrum of 5% Mn:ZnO.

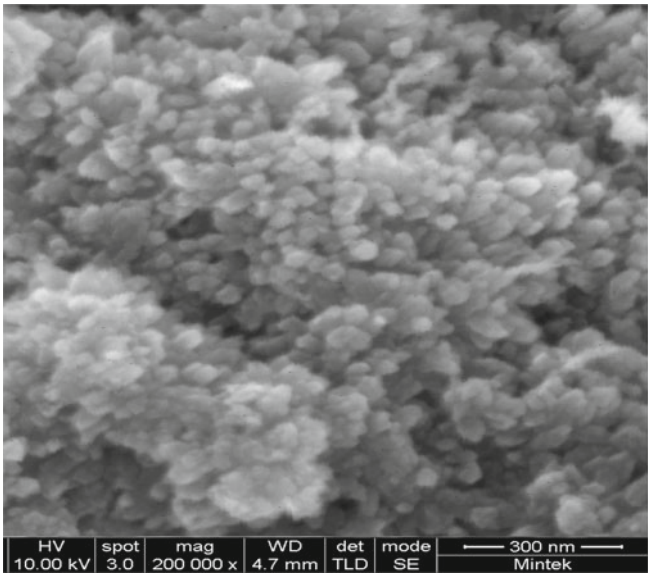

Figure 6. HRSEM image of ZnO.

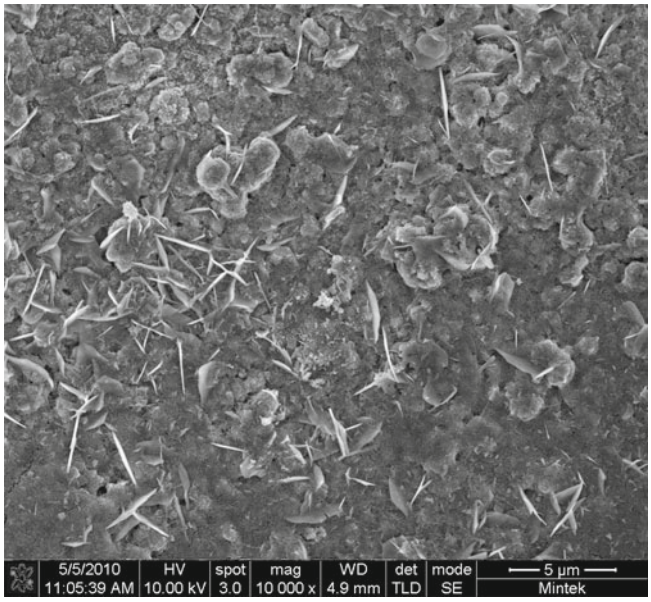

Figure 7. SEM image of 5% Mn:ZnO thin film.

The EDX spectrum confirmed the presence of Zn, O and Mn elements in the deposited films. The silicon signal possibly appears from the substrate. Dopant concentration in these two cases was 2 and 5% in the starting solution. Accordingly, the expected Mn/Zn ratio was 0·02 and 0·05 in the films. We actually obtained the Mn/Zn ratio in the films as 0·0131 and 0·0284, respectively, indicating that the amount of Mn incorporation in the film is less than the amount of Mn in the starting solution. The real Mn content in the deposited films was 1·31 and 2·84% as obtained from EDX spectrum. EDX investigations on glass and quartz substrate with increasing Mn content in the starting solution are underway.

3.3 *Optical absorption*

The optical absorbance spectrum was recorded in the wavelength range of 500–800 nm using a Shimadzu spectrophotometer-1800. Zinc oxide is a direct bandgap material (Tabet-Derraz *et al* 2002) and the energy gap (E_g) can thus be estimated by assuming direct transition between conduction bands and valence bands. Theory of optical absorption gives the relationship between the absorption coefficients, α and the photon energy, $h\nu$ as

$$\alpha h\nu = A\left(h\nu - E_g\right)^{n/2},$$

where A is a function of index of refraction and hole/electron effective masses (Pankove 1971), α the optical absorbance and 'n' a number equal to 4 for direct bandgap and 1 for the indirect bandgap semiconductors.

For our present case $n = 4$, the direct bandgap is determined using this equation, when straight portion of the $(\alpha h\nu)^2$ against $h\nu$ plot is extrapolated to intersect the energy axis at $\alpha = 0$. Figure 9 shows the dependence of optical

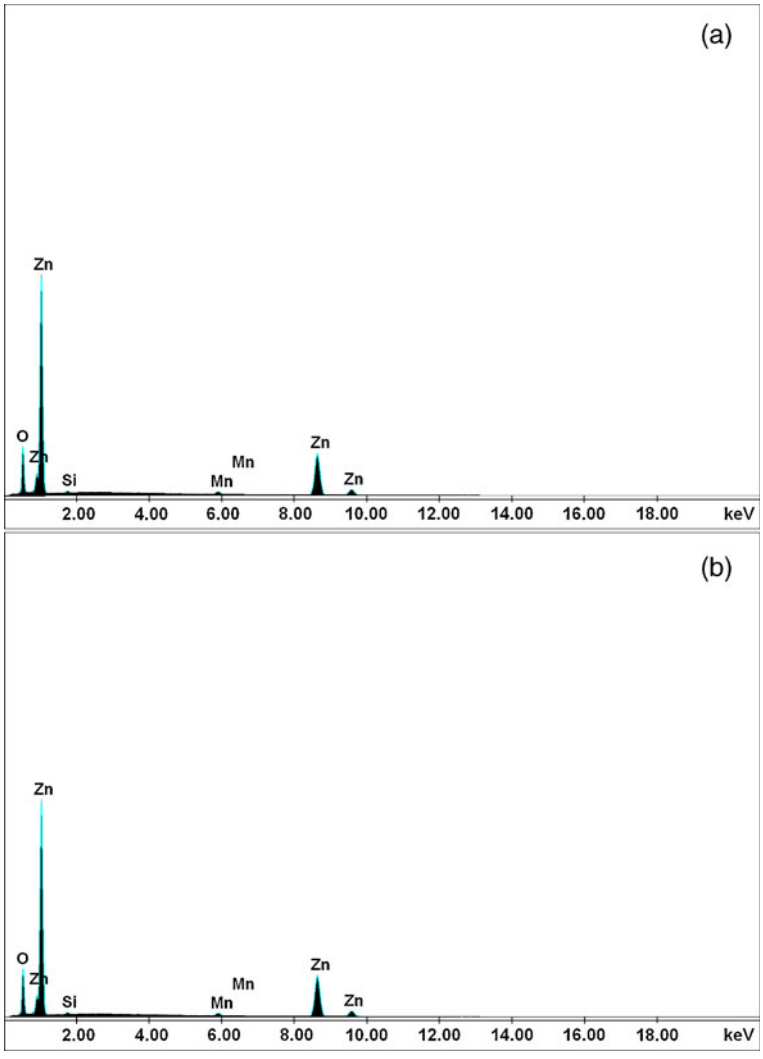

Figure 8. EDX pattern of (**a**) 2% Mn:ZnO and (**b**) 5% Mn:ZnO.

absorbance (α) on wavelength (λ). While figure 9(a) shows the dependence of α on λ for pure ZnO, figures 9(b) and (c) show dependence of α on λ for 2% Mn:ZnO and 5% Mn:ZnO, respectively. Plot of $(\alpha h\nu)^2$ against $h\nu$ for undoped and Mn-doped ZnO films was derived from figure 9 and is shown in figure 10. Figure 10(a) shows the spectrum of pure ZnO while figures 10(b) and (c) show the spectrum of 2% Mn:ZnO and 5% Mn:ZnO, respectively.

It is seen that with the increase of manganese doping level, the fundamental absorption edge decreases. The value of E_g for undoped ZnO is 3·22 eV. It decreases to 3·13 eV for 2% Mn:ZnO and 3·06 eV for 5% Mn:ZnO. The decrease in bandgap value with increased Mn doping concentration has been accounted due to the *sp-d* exchange interactions and has been theoretically explained using the second-order perturbation theory (Bylsma *et al* 1986; Singh *et al* 2009; Nirmala and Anukaliani 2010). A decrease in bandgap energy from 3·27 eV for undoped ZnO to 2·78 eV for 3% Mn-doped ZnO has been reported by Senthilkumar *et al*

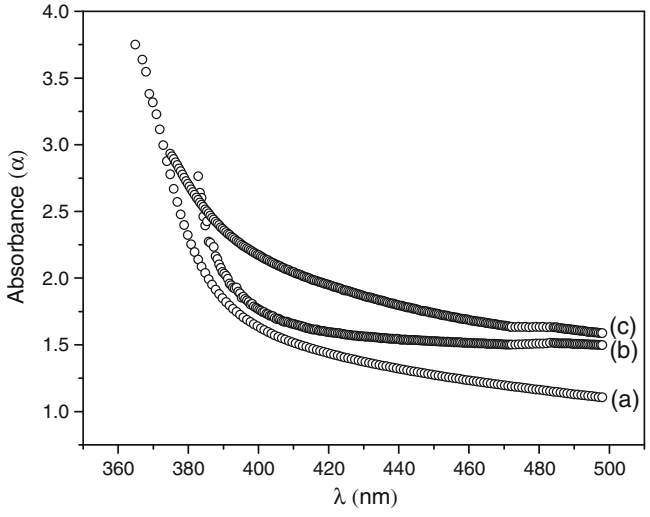

Figure 9. Plot of absorbance vs wavelength: (**a**) pure ZnO; (**b**) 2% Mn:ZnO and (**c**) 5% Mn:ZnO.

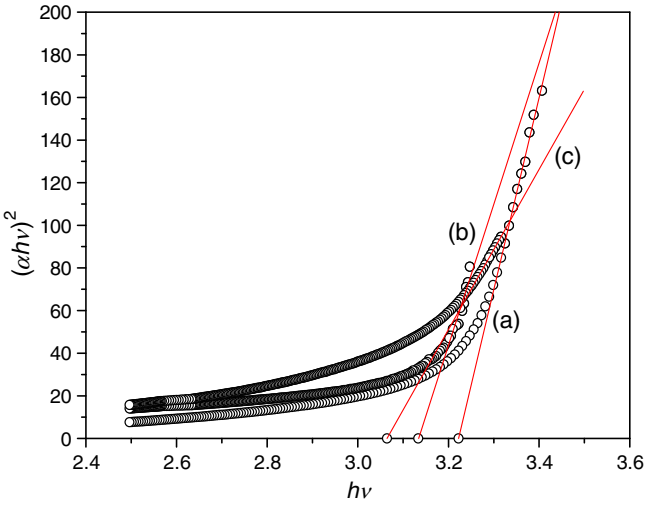

Figure 10. Plot of $(\alpha h\nu)^2$ vs $h\nu$ (in eV) for (**a**) pure ZnO; (**b**) 2% Mn:ZnO and (**c**) 5% Mn:ZnO.

(2008) and has been attributed to *s-d* and *p-d* interactions giving rise to bandgap bowing.

4. Conclusions

The primary aim of the present investigation was to explore the possibility of doping ZnO with manganese by SILAR method. Mn-doped ZnO films with different percentage of Mn content (2 and 5%) could be successfully synthesized through this technique for the first time. The films had good adherence to the substrate. Apart from being an inexpensive and simple technique, the method uses milder reaction conditions than those employed by most chemical methods proposed in the literature. Particle size is evaluated, using X-ray line broadening analysis and Williamson–Hall method shows a constantly decreasing trend with increasing manganese incorporation. The average particle size of 29·71 nm evaluated by X-ray line broadening method matches well with SEM observation. The average particle size reduces to 26·69 nm for 2% Mn:ZnO and 23·76 nm for 5% Mn:ZnO. The films are polycrystalline with an average porosity of ∼22%. The polycrystallinity of the films as well as the average microstrain increase with increasing Mn incorporation. These observations along with EDX observation confirms the replacement of zinc ions by manganese ions in the ZnO lattice. The real Mn content in the deposited film was less than that in the starting solution. Mn doping reduces fundamental absorption edge. It decreases to 3·06 eV for 5% Mn:ZnO and to 3·22 eV for pure ZnO. The materials are therefore useful for configurations that involve bandgap engineering.

Acknowledgements

One of the authors (PM) would like to acknowledge CSIR (Council of Scientific and Industrial research, New Delhi, India) for supporting the work in the form of a research project [No. 03 (1195)/11/EMR-II].

References

Bylsma R B, Becker W M, Kossut J, Debska U and Short D Y 1986 *Phys. Rev.* **B33** 8207
Choudhury N and Sarma B K 2009 *Bull. Mater. Sci.* **32** 43
Deka S and Roy P A 2007 *Solid State Commun.* **142** 190
Ghosh B, Dutta H and Pradhan S K 2009 *J. Alloys Compd.* **479** 193
Jumin X and Wang J 2001 *Mater. Lett.* **49** 318
Kale S S, Mane R S, Pathan H M, Shaikh A V, Joo O S and Han S H 2007 *Appl. Surf. Sci.* **253** 4335
Keis K, Bauer C and Boschloo G 2002 *J. Photochem. Photobiol.* **A148** 57
Klug H P and Alexander L E 1974 *X-ray diffraction procedures for polycrystalline and amorphous materials* (New York: Wiley)
Kundaliya D C *et al* 2004 *Nature Mater.* **3** 709
Look D C 2001 *Mater. Sci. Eng.* **80** 383
Luo J, Liang J K, Liu Q L, Liu F S, Zhang Y, Sun B J and Rao G H 2005 *J. Appl. Phys.* **97** 086106
Maiti U N, Ghosh P K, Ahmed F, Mitra M K and Chattopadhyay K K 2007 *J. Sol–Gel Sci. Technol.* **41** 87
Mandal S K and Nath T K 2006 *Thin Solid Films* **515** 2535
Mitra P and Khan J 2006 *Mater. Chem. Phys.* **98** 279
Mondal S, Kanta K P and Mitra P 2008 *J. Phys. Sci.* **12** 221
Mondal S and Mitra P 2012 *Bull. Mater. Sci.* **35** 751
Natsume Y 2000 *Thin Solid Films* **372** 30
Negami T, Hashimoto Y and Nishiwaki S 2001 *Sol. Energy Mater. Sol. Cells* **67** 331
Nirmala M and Anukaliani A 2010 *Photonics Letters of Poland* **2** 189
Pankove J I 1971 *Optical processes in semiconductors* (Englewood Cliffs, NJ: Prentice-Hall)
Patra S, Mitra P and Pradhan S K 2011 *Mater. Res.* (ISSN: 1516-1439) **14** 17
Senthilkumar S, Rajendran K, Banerjee S, Chini T K and Sengodan V 2008 *Mater. Sci. Semicond. Proc.* **1** 6
Sharma P *et al* 2003 *Nature Mater.* **2** 673
Singh P, Kaushal A and Kaur D 2009 *J. Alloys Compd.* **471** 11
Singhal R K, Dhawan M, Kumar S, Dolia S N, Xing Y T and Saitovitch E 2009 *Physica* **B404** 3275
Srinivasan G and Kumar J 2008 *Appl. Surf. Sci.* **254** 7285
Tabet-Derraz H, Benramdane N, Nacer D, Bouzidi A and Medles M 2002 *Sol. Energy Mater. Solar Cells* **73** 249
Ungar T and Borbely A 1996 *Appl. Phys. Lett.* **69** 3173
Wang X, Careg W P and Yee S 1995 *Sens. Actuator.* **B28** 63